Journal of Controlled Release xxx (xxxx) 1–14

Contents lists available at ScienceDirect

Journal of Controlled Release

journal homepage: www.elsevier.com/locate/jconrel

A cell-laden hydrogel as prophylactic vaccine and anti-PD-L1 amplifier against autologous tumors

Junlin Li [a], Yue Yan [a], Ping Zhang [a], Junzhou Ding [a], Yuan Huang [a], Yun Jin [b,*], Lian Li [a,*]

[a] Key Laboratory of Drug-Targeting and Drug Delivery System of the Education Ministry and Sichuan Province, Sichuan Engineering Laboratory for Plant-Sourced Drug and Sichuan Research Center for Drug Precision Industrial Technology, West China School of Pharmacy, Sichuan University, Chengdu 610041, China
[b] Sichuan Academy of Medical Sciences, Sichuan Provincial People's Hospital, Chengdu 610072, China

ARTICLE INFO

Keywords:
Orthotopic tumor model
Prophylactic vaccine
Cell-laden hydrogel
Immunotherapy
ICB therapy

ABSTRACT

Immune checkpoint blockade (ICB) can elicit anti-cancer response against tumors growing at normal organs while sparing adjacent tissues. However, many orthotopic tumors respond poorly to ICB therapy due to the lack of pre-existing immune effector cells. Here, we describe a vaccine strategy that induces protective immunity and benefits ICB therapy. An injectable hydrogel platform that forms scaffold subcutaneously was applied to deliver autologous cancer cells undergoing oncolysis (ACCO) as immunogenic antigen source and toll-like receptor 9 agonists (CpG) as additional adjuvant. When administered as a prophylactic, the hydrogel-based vaccine, denoted as (ACCO + CpG)@Gel, successfully built a durable and tumor antigen-specific immune memory against subsequent challenges with orthotopic engraftment of autologous tumors including melanoma, colon carcinoma, and lung carcinoma. Although the vaccination did not completely prevent tumor occurrence, tumors orthotopically established in vaccinated mice acquired significant enhancement in tumor-infiltrating CD8 + T cells and intratumoral PD-L1 expression, which ameliorated the immune status and rendered the originally irresponsive tumors responsible to anti-PD-L1 therapy. Further treatment with PD-L1 blockade therapy efficiently delayed the tumor growth and prolonged the survival of these orthotopic cancer models. Thus, without the need for precisely delivering immunoactivatory agents to tumor or locally remodeling tumor microenvironment, "priming" intractable or inaccessible tumors for subsequent ICB therapy could be achieved by prophylactic vaccination with (ACCO + CpG)@Gel. These findings highlighted (ACCO + CpG)@Gel as a generalized framework of protective vaccine strategy that could be broadly applicable to potentiate ICB therapy against multiple types of orthotopic tumors growing in different regions.

1. Introduction

Immune checkpoint blockade (ICB) that inhibits immune escape of tumor have revolutionized immunotherapy against various types of cancers [1–3]. Therapies that disrupt the interaction between programmed death-1 (PD-1) receptor on T cells and its ligand (PD-L1) on cancer cells can promote the recognition and killing capacity of T cells toward cancer cells [4,5], thereby eliciting durable anti-cancer immune response. Since the efficacy of ICB largely relies on immune effector cells, many patients with low tumor immunogenicity respond poorly to anti-PD-1/PD-L1 therapy due to the lack of pre-existing tumor-infiltrating T cells [6,7]. To recruit tumor-reactive T cells into tumor bed, complementary approaches including chemotherapy, radiotherapy, phototherapy, and virotherapy have been used. The rationale of most of these strategies relates to the induction of immunogenic cell death (ICD), which instigates the emission of adjuvant signals from dying cancer cells, and subsequently transforms tumors into "*in-situ* vaccine" so that the repertoire and abundance of tumor-infiltrating T cells can be increased to amplify the ICB treatment [8–12].

However, reconstructing immune landscape of tumor directly and locally requires precise delivery of ICD-inducing agents to tumor site [13,14], which poses a great challenge for treatments of microscopic tumors, especially those sporadically scattered at adjacent normal tissues. For instance, local administration of oncolytic virus to infect and lyse cancer cells is a potent approach to induce ICD [15,16], and can initiate powerful immune activation to synergize with ICB against transdermally-accessible tumors (*e.g.,* breast cancer and melanoma) [17,18]. However, to avoid systemic off-target toxicity, the virotherapy is subject to intratumoral injection [14], and not applicable for non-superficial tumors (*e.g.,* orthotopic colon and lung carcinoma) [19]. To

* Corresponding authors.
E-mail addresses: yunjin_gcp@163.com (Y. Jin), liliantripple@163.com (L. Li).

https://doi.org/10.1016/j.jconrel.2022.09.027
Received 31 May 2022; Received in revised form 11 September 2022; Accepted 12 September 2022
0168-3659/© 20XX

circumvent the need for precise drug delivery to generate *in situ* ICD in tumors, action could be taken ahead. To this end, we proposed that prophylactic vaccination with autologous cancer cells (ACC) succumbing to ICD may be an option, which could elicit tumor antigen-specific memory and then exert abscopal effect on promoting T cell infiltration into those inaccessible tumors. Despite the promise, traditional immunization strategies using ACC source often lacks potency to induce sufficient immune response, which is mainly ascribed to the low immunogenicity of whole cell lysate and its rapid degradation/elimination in the body. Recent evidences have shown that the conditions in which cells are treated impact the therapeutic function of cell-based vaccine [20,21], and the extended release of ACC permits continuous immune stimulation for amplified efficacy [22–24]. Therefore, development of effective platform that sustainably delivers highly immunogenic ACC is highly desirable.

LTX-315, with a membranolytic mode of action to induce non-viral oncolysis in cancer cells through triggering lysis/perturbation of the plasma membrane, distortion of subcellular organelles, release of damage-associated molecular patterns (DAMPs), and onset of anti-tumor immune response, is an oncolytic peptide designed for intratumoral injection and currently under phase II clinical trials [13,25–27]. We recently utilized LTX-315 to generate vaccine derived from ACC undergoing oncolysis (ACCO), which could guarantee both adjuvanticity and antigenicity: (1) secreted DAMPs functioned as "eat me" or "danger" signals to engage immune effector cells; and (2) fragments or debris from dying ACCO provided a full library of tumor-associated antigen epitopes to reduce the likelihood of tumor escape [22]. To enable sustained exposure *in vivo*, ACCO was then encapsulated into an injectable hydrogel that formed a scaffold (ACCO@Gel) at tumor resection cavity of orthotopic breast cancer model, which launched durable immune attack against postsurgical tumor residuals. Further combination with strategy that alleviated surgical trauma inflammation reversed local immunosuppression and resuscitate ACCO@Gel for effective suppression of postoperative breast cancer metastasis [22].

In this study, our aim is to investigate whether the application of ACCO@Gel, could be further extended to treatment with tumors not suitable for local drug delivery or performing surgery. Therefore, we ask two questions: (1) whether ACCO@Gel could function as protective vaccine and completely prevent the occurrence of orthotopic colon and lung carcinoma? (2) if not, whether vaccination with ACCO@Gel could "prime" the immune landscape of these intractable or inaccessible tumors to promote sequential ICB therapy? To find the answers, immunogenic ACCO antigen and immunoadjuvant CpG oligodeoxynucleotides were co-loaded in a syringeable hydrogel that formed a reservoir-like (ACCO + CpG)@Gel scaffold following subcutaneous injection to gradually release the payloads for continuous immunization. Here, CpG functioned as toll-like receptor 9 (TLR 9) agonist that could promote the activation of dendritic cells (DCs), thereby facilitating the antigen presentation for initiating T cell response [28,29]. After prophylactic vaccination with (ACCO + CpG)@Gel, the corresponding autologous tumor models of melanoma, colon carcinoma or lung carcinoma growing orthotopically were established in the vaccinated mice, followed by anti-PD-L1 therapy (Scheme 1). Notably, we found that (1) the two attributes acquired in the orthotopic tumors of (ACCO + CpG)@Gel vaccinated mice, recruitment of tumor antigen-specific T cells and enhancement of PD-L1 expression, can render the originally irresponsive tumors responsible to anti-PD-L1 therapy; (2) combination with PD-L1 blockade can unleash the function of tumor-infiltrating T cells, and further increase the anti-tumor immune response.

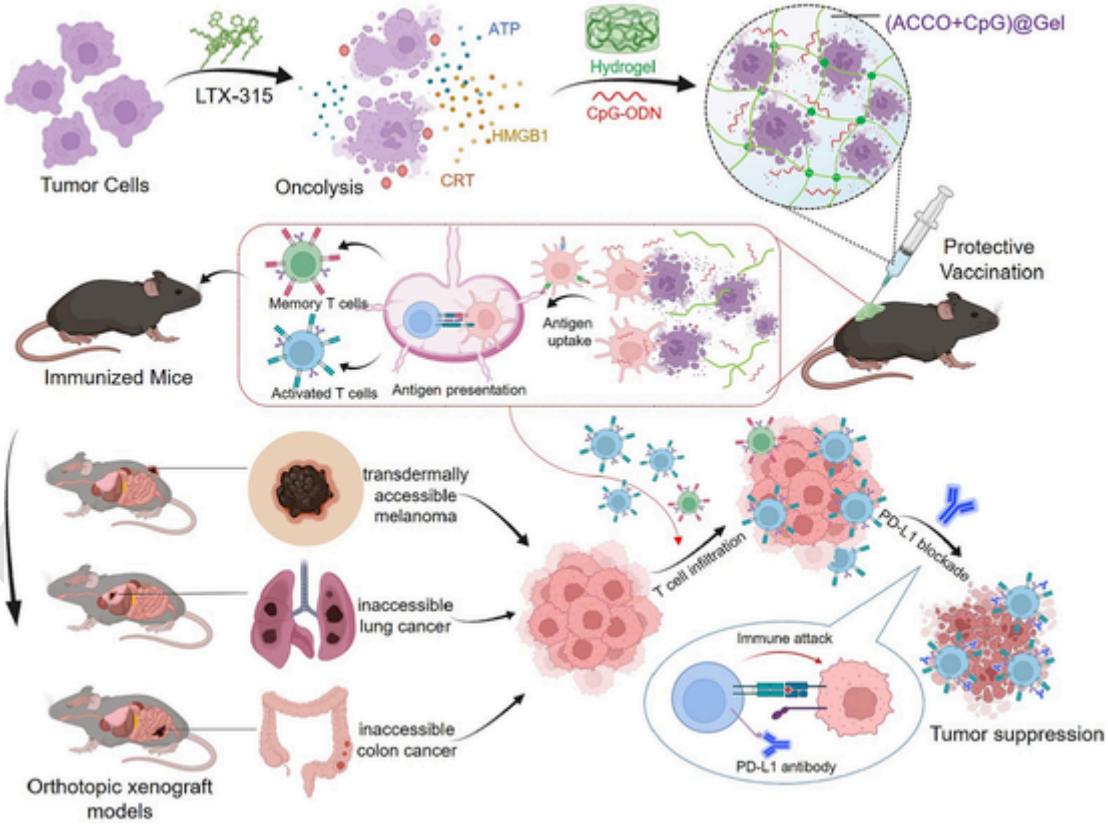

Scheme 1. Illustration of (ACCO + CpG)@Gel as protective vaccine to enhance T cell infiltration and anti-PD-L1 therapy in orthotopic model of melanoma, lung, and colon cancers.

2. Materials and methods

2.1. Cell lines and animals

B16 murine melanoma cells, CT26 murine colon cancer cells and LLC-1 Lewis lung cancer cells were purchased from Chinese Academy of Science Cell bank (Shanghai, China). B16 cells and CT26 cells were cultured in RPMI-1640 medium and LLC-1 cells were cultured in DMEM medium. All cell culture mediums were supplemented with 10% fetal bovine serum (ExCell Bio) and 1% antibiotics (penicillin and streptomycin, Beijing Solarbio Science & Technology Co.,Ltd.) Three cell lines were incubated in a 37 °C humidified environment with 5% CO_2 supply. BALB/c mice (female, 6–8 weeks) and C57BL/6 mice (female, 6–8 weeks) were purchased from Dashuo Experimental Animal Company (Chengdu, China). All of the animal experiments were approved by the Medical Ethics Committee of Sichuan University, and the animal experiments were performed in the Animal Laboratory of West China School of Pharmacy in Sichuan University (accreditation number: SYXK (Chuan)2018–113).

2.2. Preparation of ACCO and (ACCO + CpG)@Gel

To prepare ACCO, autologous tumor cells (1×10^6) were co-incubated with LTX-315 peptide (50 μM, amino acid sequence: CK-KWWKKW(*Dip*)K-NH2, Shanghai Apeptide Co., Ltd. Shanghai, China) for 4 h. Then all the cells were washed with PBS twice. Final suspension was collected as ACCO.

For the preparation of (ACCO + CpG)@Gel, ACCO (1×10^6 cells) and CpG (0.5 mg/kg, InvivoGen, the sequence: 5′-tccatgacgttcctgacgtt-3′) were suspended in 5% PVA solution (PVA; ~ 75 kDa; 99% hydrolyzed; Aladdin Biotech Co.,Ltd.) as hydrogel precursor. ROS-liable crosslinker N1-(4-boronobenzyl)-N3-(4-boronophenyl)-N1,N1,N3,N3-tetramethylpropane-1,3-diaminium (TSPBA) was synthesized as previously described [30] and further characterized by ^{1}H NMR (Fig. S1A) and mass spectrometry (Fig. S1B) showing a major peak at *m/z* 200.12 from the molecular ion peak ($C_{21}H_{34}B_2N_2O_4^{2+}$, Mw = 200.12) of TSPBA ($C_{21}H_{34}B_2Br_2N_2O_4$, Mw = 559.94). (ACCO + CpG)@Gel was formed immediately after mixing hydrogel precursor and equivalent volume of (5% wt) crosslinker TSPBA solution.

2.3. Characterization of ACCO@Gel

To investigate the morphology of PVA-based hydrogel, ACCO@Gel (100 μL) were prepared and frozen with liquid nitrogen. After lyophilization, final samples were obtained and examined by scanning electron microscope (SEM, SU3500/Aztec X-Max20). To investigate the distribution of ACCO in hydrogel, calreticulin (CRT), cytoplasm, and nucleus of ACCO was labeled with anti-CRT primary antibody/secondary Alexa Fluor 647-conjugated antibody, CellTracker Green 5-chloromethylfluorescein diacetate (CMFDA) and DAPI. The pre-stained ACCO was loaded into hydrogel and detected by confocal microscope (CLSM, Zeiss LSM 510 DUE, Jena, Germany). The dynamic rheological behavior of ACCO@Gel was measured using a TA Instruments AR 2000 rheometer at 25 °C with angular frequency and oscillation frequency from 0.1 to 10 rad/s. Then cytoplasm and nucleus were labeled with CellTracker Green 5-chloromethylfluorescein diacetate (CMFDA, 25 °C, 30 min) and 4′,6-diamidino-2-phenylindole (DAPI, 25 °C, 5 min). Afterward, the three-dimensional construction image was examined by Confocal Laser Scanning Microscopy (CLSM, LSM 700, Carl Zeiss, Jena, Germany).

To investigate the degradation of hydrogel *in vivo*, 4 nmol cyanine 5 (Cy5, Meilunbio, Dalian, China) was loaded into 50 μL PVA solution and further crosslinked with equal volume of TSPBA solution (5% wt) to form Cy5@Gel. Then C57BL/6 mice were subcutaneously injected with 100 μL Cy5 solution or Cy5@Gel and their fluorescence images were acquired on day 0, 3, 7, 14 by an IVIS Spectrum *In Vivo* Imaging System (PerkinElmer, Lumina 3).

2.4. Oncolytic peptide LTX-315 induced ICD of three kinds of tumor cells

To confirm the stimulation of ICD in B16 cells, CT26 cells and LLC-1 cells after treatments with LTX-315 peptide, CRT as hallmark of ICD was investigated by confocal microscope imaging and flow cytometry. First, B16 cells, CT26 cells, and LLC-1 cells were treated with LTX-315 peptide (50 μM) for 4 h, washed twice with PBS to obtain ACCO, and then ACCO was incubated with fresh culture medium for 24 h prior to ICD detection. ACCO was blocked with 5% goat serum, incubated with CRT primary antibody (1:500, abcam, ab2907) at 4 °C for 1 h, washed with PBS, further incubated with secondary Alexa Fluor 647-conjugated antibody (1:1000, ab150077) and analyzed by flow cytometry. For fluorescence imaging measurement, CRT on the ACCO surface was stained *via* the same method. Another two ICD-associated DAMPs, adenosine triphosphate (ATP) and high mobility group protein B1 (HMGB1) were also detected. To quantify the ATP secretion, the supernatant of ACCO suspension was collected and ATP concentration was detected by ATP Assay Kit (Beyotime S0026). Meanwhile, released HMGB1 was detected by Western blot according to the protocol as previously reported [31].

2.5. (ACCO + CpG)@Gel vaccination against melanoma

In murine melanoma model, ACCO@Gel and (ACCO + CpG)@Gel derived from B16 cells were injected subcutaneously in C57BL/6 twice on day −28 and − 14 as pre-vaccination. Meanwhile, body weights of mice were recorded every three days. On day 0, B16 cells (5×10^5) were subcutaneously injected to establish the melanoma tumor model. Three doses of anti-mouse α-PD-L1 antibody (100 μg or 200 μg per mouse; Clone: 10F.9G2; BioXcell) were intraperitoneally administered at day 6, 8, and 10 after tumor cell inoculation. Tumor size and animal survival were recorded every other day and tumor volume was calculated as follows: tumor volume (mm^3) = 1/2 × width^2 × length. In another individual experiment, mice were sacrificed on day 17, and tumor tissues and spleens were harvested for immune status analysis. To obtain the single cell suspension, tumor-draining lymph nodes were dissociated in digestion buffer, ground, and filtered through a 70 μm nylon strainer. For the detection of CD80 + CD86 + CD11c + activated DCs, cells were blocked with anti-CD16/32 antibody at 4 °C for 30 min, and stained with anti-CD11c-FITC (1:400 dilution), anti-CD80-PE (1:400 dilution), and anti-CD86-PerCP-Cy5.5 (1:400 dilution) at 4 °C for 1 h. Afterward, cells were washed twice with PBS and analyzed by flow cytometry. Similarly, single cell suspensions from tumors and spleens were prepared in the same way and red blood cells were lysed with ACK lysis buffer (4 °C, 10 min, Thermo Scientific). To further assess CD8+ T cells in tumor, cells were pre-blocked with anti-CD16/32 antibody, stained with anti-CD3-FITC (1:400 dilution), anti-CD8-APC (1:400 dilution), anti-CD4-PerCP-Cy5.5 (1:400 dilution), and further analyzed by flow cytometry. To investigate the formation of durable immunity, single cell suspensions isolated from spleens were fixed, pre-blocked, and stained with anti-CD62L-PerCP-Cy5.5 (1:300 dilution), anti-CD44-PE (1:300 dilution), and anti-CD8-APC (1:300 dilution) antibodies as described above.

2.6. (ACCO + CpG)@Gel elicited antigen-specific response against melanoma

In another individual experiment, CCO was made from non-autologous tumor cells (CT26 cells or LLC-1 cells) while ACCO was derived from autologous murine B16 cells. C57BL/6 mice were pre-vaccinated twice with CCO_{CT26}, CCO_{LLC-1}, or $ACCO_{B16}$, respectively. After two doses of vaccine administration, mouse skin attached to the hydrogel was collected and fixed with 4% paraformaldehyde for H&E staining analysis. Meanwhile, body weights of mice during vaccination were recorded every 3 days. On day 0, B16 cells (5×10^5) were subcutaneously injected to establish the melanoma tumor model followed by three doses of α-PD-L1 antibody (100 μg or 200 μg per mouse) therapy. Tumor volumes were calculated as described above and recorded every other day. For the detection of tumor immune microenvironment, mice were sacrificed and tumors were collected at the end point (day 21). Single cell suspension was obtained as mentioned above and supernatant was collected at the same time. For the analysis of tumor infiltration of CD3 + CD8+ T cells, tumor cells were fixed, pre-blocked, stained with anti-CD3-FITC, anti-CD8-APC, anti-CD4-PerCP-Cy5.5, and washed again for flow cytometry. Intratumoral concentration of IFN-γ in cell suspension before ACK lysing was detected by mouse IFN-γ ELISA kit (Quanzhou Ruixin Biological Technology Co., Ltd., Quanzhou, China).

2.7. (ACCO + CpG)@Gel→α-PD-L1 against orthotopic colon carcinoma

In orthotopic colon cancer model, ACCO was prepared from autologous CT26 cells. After two doses of (ACCO + CpG)@Gel vaccination, orthotopic colon cancer model was established as follows: 8-week-old female BALB/c mice were anesthetized with 5% chloral hydrate (120 μL) and placed in the supine position in a sterile environment. For colonic tumor inoculation, a midline incision was made to expose the colon location after abdominal hair was shaved. CT26 cells (8×10^5 cells in 100 μL PBS) were injected into the colonic mucosa and the injection site was pressed immediately to prevent cell suspension leakage. Then the colon was gently returned to the abdominal cavity. Entire process required aseptic manipulation. Subsequential three doses of α-PD-L1 antibody (100 μg or 200 μg per mouse) were intraperitoneally injected at day 2, 4, and 6. Meanwhile, animal survival was recorded every day. In another individual experiment, mice were sacrificed at day 10 for the analysis of immune activation induced by vaccines. Colon cancer was isolated, photographed, and further fixed with 4% paraformaldehyde for hematoxylin–eosin staining and immumohistochemical (CD8 and IFN-γ) staining analysis. Meanwhile, Lymph nodes were collected and homogenized to single cell suspension by the same method mentioned above. For the measurement of CD80 + CD86 + CD11c + matured DCs, cells from lymph node were fixed, blocked, stained with anti-CD11c-FITC, anti-CD80-PE, anti-CD86-PerCP-Cy5.5, and followed by flow cytometry. For the analysis of CD8 + CD62L-CD44+ effector memory T cells, single cell suspension from spleens was prepared as described above and stained with anti-CD8-APC, anti-CD44-PE and anti-CD62L-PerCP-Cy5.5, followed by flow cytometry.

2.8. (ACCO + CpG)@Gel→α-PD-L1 against LLC-1 Lewis lung carcinoma

In LLC-1 Lewis lung cancer model, ACCO was prepared from autologous LLC-1 cells. With two doses of (ACCO + CpG)@Gel vaccination on day −28 and day −14, LLC-1 cells (1×10^6) were intravenously injected into C57BL/6 mice on day 0 to establish orthotopic Lewis lung cancer. Then three doses of α-PD-L1 antibody (100 μg or 200 μg per mouse) were intraperitoneally administrated on day 6, 8, and 10. Body weights during vaccination and survival time were recorded. In another individual experiment, mice were sacrificed at the end point (day 16). Lungs were collected, photographed, and further fixed with 4% paraformaldehyde for hematoxylin–eosin and immumohistochemical (CD8) staining analysis. Meanwhile, lymph nodes, and spleens were harvested and prepared as single cell suspension as described above. For the detection of CD80 + CD86 + CD11c + matured DCs, cells from lymph node were fixed, pre-blocked, stained with anti-CD11c-FITC, anti-CD80-PE, anti-CD86-PerCP-Cy5.5, and washed again for flow cytometry analysis. Splenic effector memory T cells were analyzed as described above.

2.9. Statistical analysis

Data was presented as means ± standard deviations (SD). Statistical significance between two or more groups was calculated by student's *t*-test or one-way analysis of variance (ANOVA). Statistical analysis was performed using Graphpad Prism 8.0 software.

3. Results and discussion

3.1. Emission of ICD-associated DAMPs in ACCO

In this study, ACCO derived from murine B16 melanoma cells, CT26 colon carcinoma cells, and LLC-1 lung carcinoma cells were generated by treating B16, CT26, and LLC-1 cells with oncolytic LTX-315, respectively, for 4 h. Afterward, ACCO was obtained by washing and collecting these LTX-315-treated dying cells. To investigate whether there was an increment in the immunogenicity of ACCO and whether the increment could remain for a period of time, ICD-associated DAMPs hallmarks (*i.e.,* surface exposure of CRT, extracellular secretion of ATP, and release of HMGB1) were analyzed after B16, CT26, or LLC-1 cell-derived ACCO was suspended in fresh culture medium for another 24 h. Confocal microscopy showed that, as compared with naïve cancer cells, the ACCO derived from all three cell lines showed abundant CRT exposure. Flow cytometry analysis further confirmed that the percentage of surface CRT-positive B16, CT26, and LLC-1 cells reached approximately 66%, 56% and 53% within the ACCO, respectively, whereas that was minimally below 3% in naïve cells (Fig. 1A). In addition, ATP detection in culture supernatant showed an identical trend that ACCO had considerably increased ATP secretion (Fig. 1B). As expected, western bolt also showed that ACCO had substantially higher release of HMGB1 extracellularly than naïve cells (Fig. 1C). These results validated that, even after LTX-315 treatment had been ceased and cells had been washed, the obtained ACCO derived from B16 melanoma cell, CT26 colon carcinoma cells, and LLC-1 lung carcinoma cells continuously emitted self-adjuvanting signals of massive ICD associated DAMPs (Fig. S2).

3.2. Characterization of ACCO@Gel

To prolong the exposure time of bioactive ACCO *in vivo*, a hydrogel platform [32,33] was applied for the extended delivery. The hydrogel scaffold harboring ACCO (ACCO@Gel) could be formed promptly by the injection of the mixture of ACCO-loaded polyvinyl alcohol (PVA) solution as the hydrogel precursor and TSPBA solution as the crosslinker (Fig. 2A) [22,30].

Scanning electron microscopy imaging (Fig. 2B) showed that blank hydrogel after crosslinking had compact polymer network structure with interconnected pores, which was obviously different from the loose morphology of hydrogel precursor without crosslinking. Meanwhile, after ACCO encapsulation, a large number of ACCO tightly filled the voids of the hydrogel, and distributed uniformly within ACCO@Gel. In consistence, 3D scanning using confocal microscopy also revealed that ACCO with CRT surrounded dispersed uniformly in ACCO@Gel (Fig. 2C). The result suggested that the hydrogel had the ability to maintain both cellular antigens and adjuvantic DAMPs. In addition, mechanical analysis for ACCO@Gel using rheological measurements (Fig. 2D) confirmed its gelatinous property, as evidenced by the storage

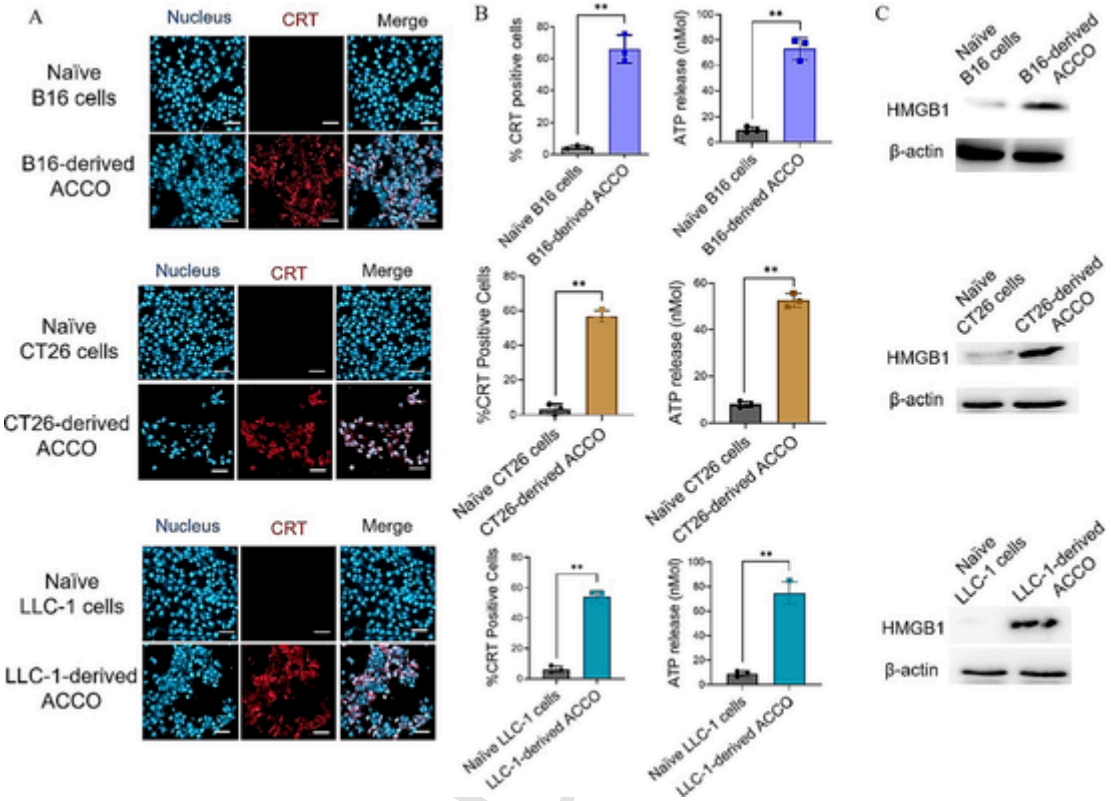

Fig. 1. ACCO derived from murine B16 melanoma cells, CT26 colon carcinoma cells, and LLC-1 lung carcinoma cells were obtained by incubating the cancer cells with LTX-315 peptide for 4 h followed by PBS washing, and then ACCO was suspended in fresh culture medium for another 24 h before investigating whether ACCO could continuously emitted ICD associated DAMPs including (A) surface CRT exposure, (B) extracellular ATP secretion, and (C) extracellular HMGB1 release. The data are presented as mean ± SD, $n = 3$, $^{**}p < 0.01$.

modulus (G') drastically larger than the loss modulus (G"). The strain sweep measurements revealed that the linear viscoelastic region of the hydrogel reached 10% of the oscillation strain, indicating its viscoelastic property. Rheological analysis also confirmed the hydrogel formation of the final products of ($ACCO_{B16}$ + CpG)@Gel, ($ACCO_{CT26}$ + CpG)@Gel, and ($ACCO_{LLC-1}$ + CpG)@Gel (Fig. S3). As shown in Fig. 2E, (ACCO + CpG)@Gel degraded gradually at a relatively slower rate in PBS medium at physiological pH 7.4, while an accelerated degradation of (ACCO + CpG)@Gel occurred under ROS condition (pH 7.4 PBS + 1 mM H_2O_2) because the pinacol esters formed between the hydrogel precursors and TSPBA crosslinkers were ROS-liable [30]. In addition, (ACCO + CpG)@Gel could gradually degrade and sustainably release the cargos over 7 days. The release of payload from the hydrogel highly correlated with the hydrogel degradation. The profile of ACCO release almost overlapped with the profile of (ACCO + CpG)@Gel degradation; meanwhile, CpG was also released as (ACCO + CpG)@Gel degraded but exhibited a relatively slower pattern as compared with ACCO. As ACCO with a larger cellular size mainly localizes in the larger porous structure or channel of the hydrogel, we anticipated that once the hydrogel disintegrates, ACCO can more readily leak out, making ACCO release degradation-controlled.

Next, we investigated the retention of hydrogel at the subcutaneous injection site. Free fluorescent Cy5 solution and Cy5-loaded hydrogel (Cy5@Gel) were injected subcutaneously in mice. Optical images of mice were acquired using an *In Vivo* Imaging System IVIS at the predetermined time points (Fig. 2F). Results showed that free Cy5 had a fast clearance within 3 days. Obvious signal of Cy5@Gel could last for over 7 days after subcutaneous injection in mice, suggesting that hydrogel degraded eventually at physiological environment and prolonged retention time to extend ACCO exposure. There is a little inconsistence that the hydrogel degraded faster *in vitro* than *in vivo*, because for *in vitro* experiment (ACCO + CpG)@Gel was immersed in aqueous solution while for *in vivo* degradation the fluid in subcutaneous injecting site was not as that much to completely cover the hydrogel scaffold. Although the *in vitro* condition did not fully recapitulate *in vivo* condition, these results together demonstrated that (ACCO + CpG)@Gel gradually degraded and sustainably released the cargos. A similar phenomenon was also observed in our previous work [22]. Moreover, histology analysis of local skin tissues adhered by various (ACCO + CpG)@Gels showed no tissue toxicity or apparent inflammatory cell infiltration as the hydrogel degraded and release the payloads (Fig. 2G).

3.3. (ACCO + CpG)@Gel vaccination against melanoma

We first investigated the effect of (ACCO + CpG)@Gel as protective vaccine on preventing the melanoma in C57BL/6 mice. Mice were pre-vaccinated with two subcutaneous injections of blank hydrogel, ACCO@Gel derived from B16 cells, or (ACCO + CpG)@Gel, and then challenged with subcutaneous inoculation of B16 melanoma cells, following the monitor of tumor occurrence and growth until the immunology analysis (Fig. 3A). Results of overall (Fig. 3B) and individual (Fig. 3C) tumor growth curves showed that both ACCO@Gel and (ACCO + CpG)@Gel failed to completely prevent the melanoma occurrence, but they did slow down the tumor progression as compared with the blank control. As compared with the blank control (21 days), the median survival time of ACCO@Gel and (ACCO + CpG)@Gel groups extended to 29.5 and 43 days, respectively (Fig. 3D).

At the endpoint, mice were sacrificed, and various tissues were collected for immunology analysis. As shown in Fig. 3E, as compared with the blank control, ACCO@Gel induced significantly higher frequencies of mature CD80 + CD86 + CD11c + DCs in tumor, lymph nodes, and spleens, probably because ACCO had massive exposure of ICD-associated DAMPs as self-adjuvanting signals that facilitated the antigen engulfment and DC maturation. Meanwhile, because of the addi-

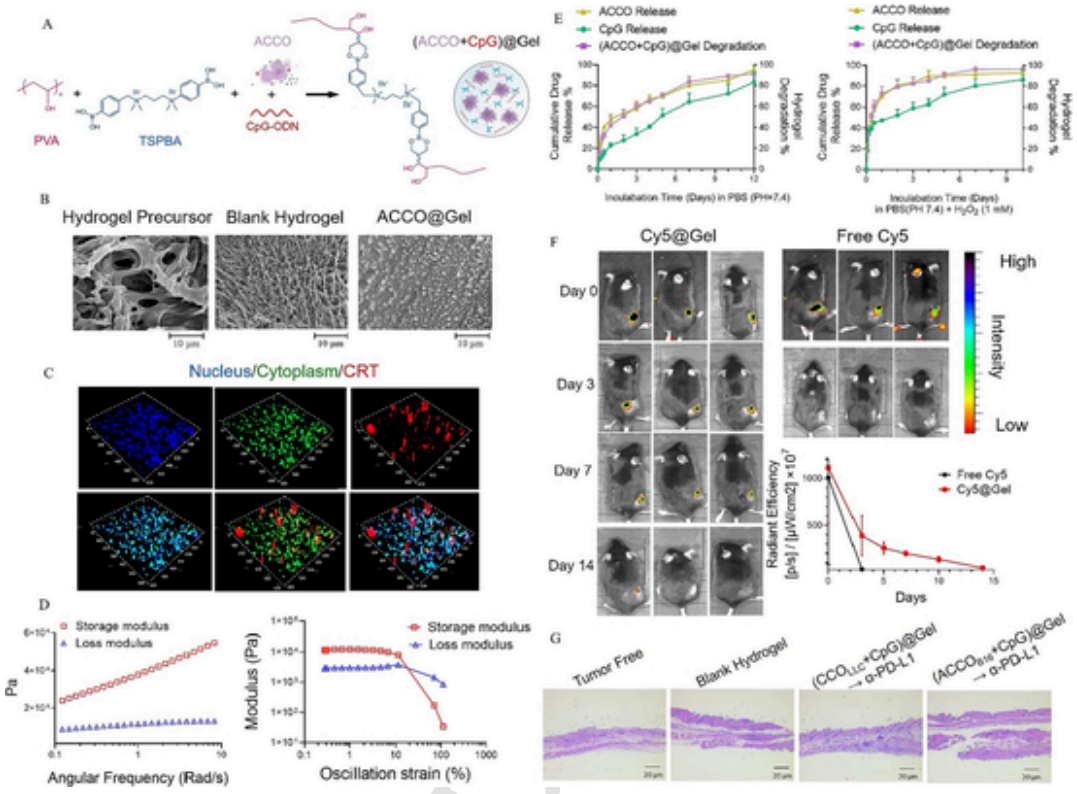

Fig. 2. Characterization of ACCO@Gel. (A) Schematic diagram of (ACCO + CpG)@Gel formation after the dual phenylboronic acids of TSPBA crosslinker spontaneously and rapidly react with diols on PVA to form degradable pinacol ester. (B) SEM images of hydrogel precursor, blank hydrogel and ACCO@Gel. (C) Three-dimensional construction images of hydrogel encapsulating pre-stained ACCO: CRT (red), cytoplasm (green), nucleus (blue). (D) Frequency-dependent rheological properties of ACCO@Gel and strain sweep dynamic rheological data for ACCO@Gel (ω = 1 rad/s). (E) ACCO and CpG release from hydrogel and the correlation with (ACCO + CpG)@Gel degradation in PBS (pH 7.4) medium with or without H_2O_2 (1 mM). (F) *In vivo* degradation of Free Cy5 and Cy5@Gel in C57BL/6 mice model and average quantitative fluorescent signals of Cy5 (n = 3). (G) H&E staining image of skin tissue attached to hydrogel vaccine derived from various tumor cells. Scale bar, 20 μm. (For interpretation of the references to colour in this figure legend, the reader is referred to the web version of this article.)

tional function of CpG adjuvant, DC activation was further improved by (ACCO + CpG)@Gel. Consequently, tumors in ACCO@Gel vaccinated mice were infiltrated with a significantly higher number of both CD3 + CD8+ and CD3 + CD4+ T cells than blank hydrogel control, because of the immunization effect. Interestingly, as compared with blank hydrogel, ACCO@Gel vaccination resulted in a drastically increased percentage of CD8+ T cells in CD3+ T cells, but a slightly decreased percentage of CD4+ T cells in CD3+ T cells within the tumors (Fig. 3F). While CD8+ T cells could exert direct killing effect on cancer cells, the role of CD4+ T cells was complicated, which could be divided into effective T cells that are helpful to promote immune responses and Foxp3+ regulatory T cells (Tregs) that are immunosuppressive. This finding demonstrated that ACCO@Gel vaccination recruited CD3+ T cells into tumors with an increased proportion of CD8+ T cells to CD4+ T cells, indicating a more straightforward anti-tumor immune response. Furthermore, (ACCO + CpG)@Gel showed superior effect over ACCO@Gel on increasing the frequency of tumor-infiltrating CD8+ T cells (Fig. 3F), suggesting the CpG adjuvant contributed additional immunoactivatory effect.

Collectively, the tumor inhibition capability of ACCO@Gel could be ascribed to the immunization effect of immunogenic ACCO, and the better capability of (ACCO + CpG)@Gel could be ascribed to additional immune activation by CpG adjuvant. Although (ACCO + CpG)@Gel vaccination was unable to prevent the melanoma occurrence, but it could improve the tumor immune status by effectively increasing the tumor infiltration of CD8+ T cells, which may be beneficial to subsequent therapy of ICB.

3.4. Potentiation of anti-PD-L1 therapy

We next investigated whether (ACCO + CpG)@Gel could potentiate anti-PD-L1 therapy in melanoma mice. We observed that tumoral PD-L1 expression was upregulated in the orthotopic melanoma tumor model that had been vaccinated with (ACCO + CpG)@Gel (Fig. 4A). Given the recruitment of CD8+ T cells in the tumor of (ACCO + CpG)@Gel-vaccinated mice (Fig. 3F), the enhancement of tumoral PD-L1 expression could be due to a negative feedback response from cancer cells to escape immune attack [9,11]. This finding highlighted the necessity of further combining with PD-L1 blockade. After (ACCO + CpG)@Gel vaccination and tumor challenge as described above, mice with occurrent melanoma received three doses of anti-PD-L1 monoclonal antibody (α-PD-L1) intraperitoneally (Fig. 4A). As shown in Fig. 4B and C, mice responded poorly to α-PD-L1 alone, and had barely improved median survival time of 23.5 days. This could be attributed to the deficiency of tumor-infiltrating T cells (Fig. 4D). By comparison, in (ACCO + CpG)@Gel vaccinated mice, α-PD-L1 significantly inhibited the tumor growth, and further extended the median survival time to over 60 days (Fig. 4B and C), which may be the result of substantial recruitment of T cells in tumors (Fig. 4D). To demonstrate the recruited CD8+ T cells were also tumor reactive, we next investigated the amount of IFN-γ and TNF-α secreting CD8+ T cells in tumors of (ACCO + CpG)@Gel vaccinated mice receiving α-PD-L1 therapy (Fig. 4E). Both quantitative results using flow cytometry and qualitative results using confocal microscopy showed that, as compared with blank hydrogel group, α-PD-L1 alone failed to upregulate the level of intratumoral TNF-α or IFN-γ due to the deficiency in tumor-infiltrating CD8+ T cells. With the immunization effect induced by ACCO and additional CpG adjuvant,

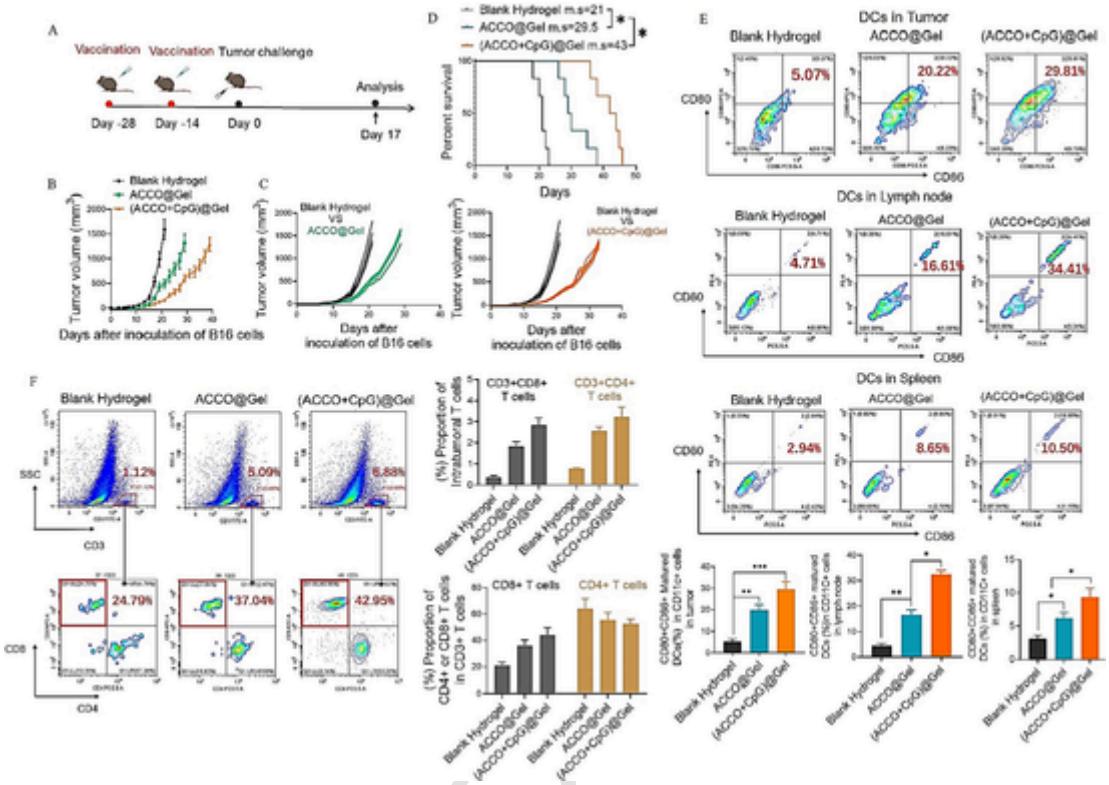

Fig. 3. (ACCO + CpG)@Gel as protective vaccine suppresses the growth of melanoma. (A) Schedule for the vaccination with (ACCO + CpG)@Gel in C57BL/6 mice model. Overall (B) and individual (C) growth curves of tumor in mice pre-vaccinated with blank hydrogel, ACCO@Gel and (ACCO + CpG)@Gel (n = 6). (D) Survival curves for the blank hydrogel and vaccines treated mice (n = 6). (E) Frequencies of CD80 + CD86 + CD11C+ matured DCs in tumor, lymph node, spleen and (F) CD3 + CD4+ T cells and CD3 + CD8+ T cells in vaccinated mice at the end point (n = 6). Statistical analysis was performed using one-way ANOVA; $^{*}p < 0.05$, $^{**}p < 0.01$, $^{***}p < 0.001$.

(ACCO + CpG)@Gel promoted CD8+ T cell infiltration but only induced limited secretion of TNF-α and IFN-γ, probably due to the observed enrichment of intratumoral PD-L1 (Fig. 4A) that deactivate the CD8+ T cells. Notably, after sequential PD-L1 blockade in (ACCO + CpG)@Gel-vaccinated mice, (ACCO + CpG)@Gel→α-PD-L1 resulted in significantly increased frequencies of TNF-α + CD8+ and IFN-γ + CD8+ tumor-reactive T cells. Thus, (ACCO + CpG)@Gel vaccination and α-PD-L1 blockade could only work collaboratively to elicit stronger anti-tumor immune response than any strategy used alone. Furthermore, as compared with blank hydrogel and α-PD-L1 monotherapy, ACCO vaccination-based therapies including ACCO@Gel, (ACCO + CpG)@Gel and (ACCO + CpG)@Gel→α-PD-L1 significantly enlarged the frequency of splenic CD44 + CD62L- memory effect T cells (Fig. 4F), indicating the establishment of durable immunity. These results verified that (ACCO + CpG)@Gel as the protective vaccine could potentiate anti-PD-L1 therapy against melanoma by shaping the tumor immunity.

3.5. Elicitation of tumor antigen-specific immune memory

To demonstrate whether the elicitation of anti-tumor memory is tumor type specific, we prepared the ($ACCO_{B16}$ + CpG)@Gel vaccine derived from autologous B16 cells undergoing oncolysis, and (CCO_{CT26} + CpG)@Gel and (CCO_{LLC-1} + CpG)@Gel vaccines derived from heterologous CT26 cells and LLC-1 cells against B16 melanoma *in vivo* following an identical schedule in Fig. 4A. As compared with blank hydrogel, sequential (CCO_{CT26} + CpG)@Gel/(CCO_{LLC-1} + CpG)@Gel vaccination and anti-PD-L1 therapy exhibited limited effect on suppressing the growth of melanoma (Fig. 5A). By comparison, consecutive treatments with ($ACCO_{B16}$ + CpG)@Gel and α-PD-L1 significantly inhibited the growth of cognate tumor, which also showed better therapeutic outcome against the melanoma than ($ACCO_{B16}$ + CpG)@Gel. In another individual experiment, ($ACCO_{B16}$ + CpG)@Gel-vaccinated mice were concurrently treated with α-PD-L1 and CD8+ T cell depleting antibody. As shown in Fig. 5B, ($ACCO_{B16}$ + CpG)@Gel→α-PD-L1 exerted reproducible anti-tumor effect and still considerably inhibited the growth of B16 melanoma. However, such promising effect were drastically contradicted by additional CD8+ T cell depletion, resulting in a similar effect with (CCO_{CT26} + CpG)@Gel→α-PD-L1 which merely retarded the tumor progression. This result demonstrated that (ACCO + CpG)@Gel→α-PD-L1 exerted anti-tumor effect largely through CD8+ T cell activation. Indeed, ($ACCO_{B16}$ + CpG)@Gel→α-PD-L1 significantly promoted the intratumoral infiltration of CD3+ and CD8+ T cells in the melanoma, whereas the effect of (CCO_{CT26} + CpG)@Gel/(CCO_{LLC-1} + CpG)@Gel→α-PD-L1 was moderate (Fig. 5C). Since tumor-reactive T cells elicits tumor-killing effect by producing cytokines like IFN-γ [34], we then investigated the intratumoral concentration of IFN-γ after various treatments (Fig. 5D). In a similar trend, melanoma did not respond to (CCO_{CT26} + CpG)@Gel/(CCO_{LLC-1} + CpG)@Gel→ α-PD-L1. In contrast, significantly higher amount of IFN-γ was secreted in the melanoma of mice treated with ($ACCO_{B16}$ + CpG)@Gel→α-PD-L1. In addition, ($ACCO_{B16}$ + CpG)@Gel also increased the intratumoral concentration of IFN-γ because of the immunization effect, but had less potency than ($ACCO_{B16}$ + CpG)@Gel→α-PD-L1. To further demonstrate the induction of tumor-antigen-specific CD8+ T cells, we also quantitatively and qualitatively compared the amounts of TNF-α + CD8+ T cells and IFN-γ + CD8+ T cells in tumors of mice vaccinated with non-autologous cancer derived vaccine (CCO_{CT26} + CpG)@Gel and autologous cancer cell derived vaccine ($ACCO_{B16}$ + CpG)@Gel. As shown in Fig. 5E, as compared with (CCO_{CT26} + CpG)@Gel→α-PD-L1, ($ACCO_{B16}$ + CpG)@Gel→α-PD-L1 induced significantly higher tumor

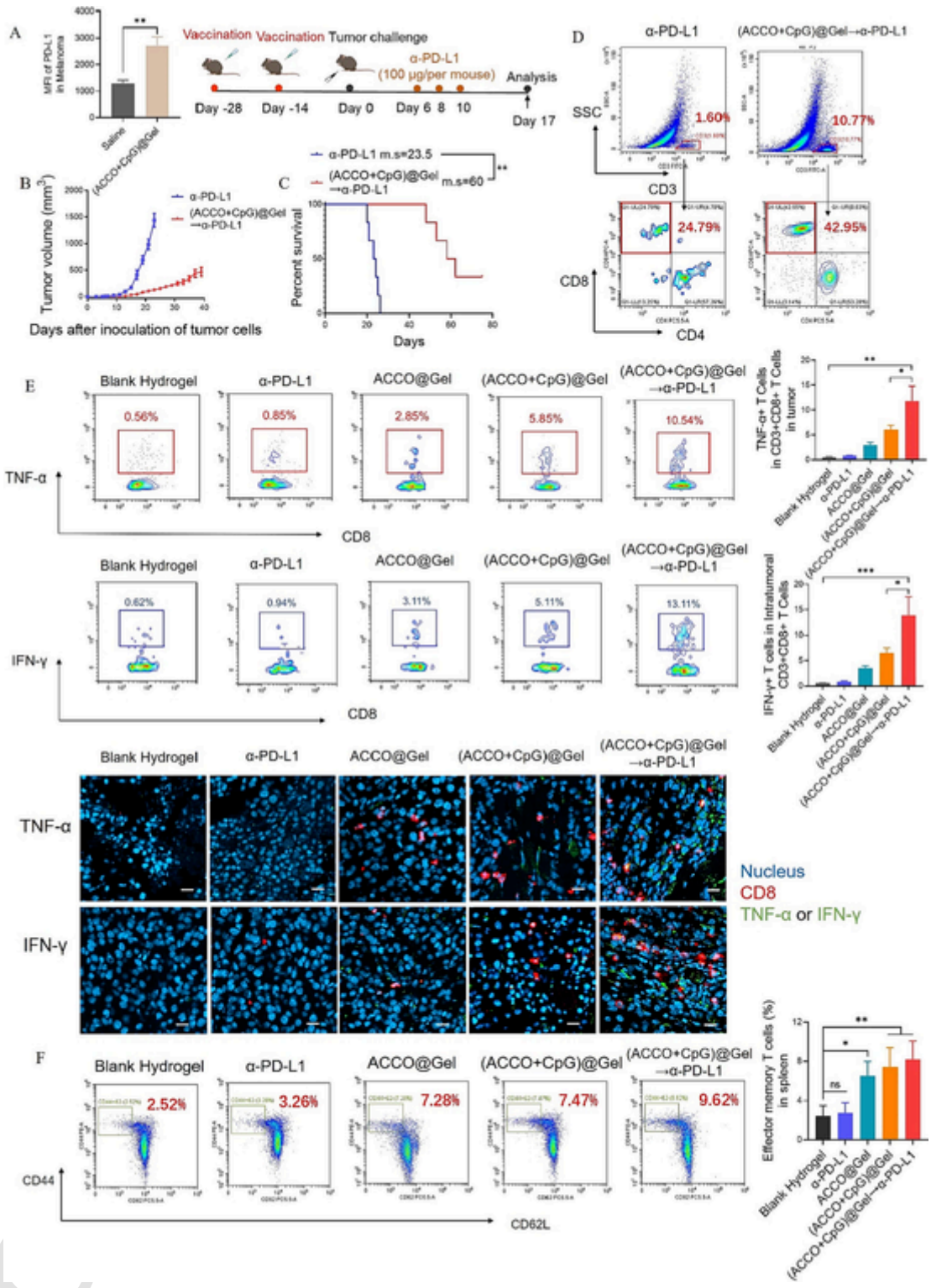

Fig. 4. (ACCO + CpG)@Gel potentiate α-PD-L1 therapy. (A) Intratumoral PD-L1 expression in vaccinated mice in melanoma cancer model ($n = 6$) and schedule for pre-vaccination of (ACCO + CpG)@Gel and sequential injection of three doses of anti-PD-L1 antibody in C57BL/6 mice. (B) Tumor growth curves of tumor in mice treated with α-PD-L1 and (ACCO + CpG)@Gel→α-PD-L1 (n = 6). (C) Survival curves of mice treated with α-PD-L1 and (ACCO + CpG)@Gel→α-PD-L1 (n = 6). (D) Flow cytometry plots of tumor-infiltrating CD3+ T cells and CD3 + CD8+ T cells in mice at the end point ($n = 6$). (E) Flow cytometry analysis and immunofluorescence staining of CD8 + TNF-α + T cells and CD8 + IFN-γ + T cells in tumor (Scale bar, 20 μm). (F) Flow cytometry plots and proportions of effector memory T cells in the spleen (gated on CD8+). Statistical analysis was performed using one-way ANOVA; $^{*}p < 0.05$, $^{**}p < 0.01$, $^{***}p < 0.001$.

infiltration of TNF-α + CD8+ T cells and IFN-γ + CD8+ T cells that were reactive to B16 melanoma. These results highlighted that: (1) (ACCO + CpG)@Gel vaccination could make autologous tumors, but not heterologous tumors, response positively to anti-PD-L1 therapy by eliciting tumor antigen-specific immune activation; (2) α-PD-L1 could function as the amplifier of the anti-tumor immunity by unleashing the T cells which were recruited into tumors as the result of (ACCO + CpG)@Gel vaccination.

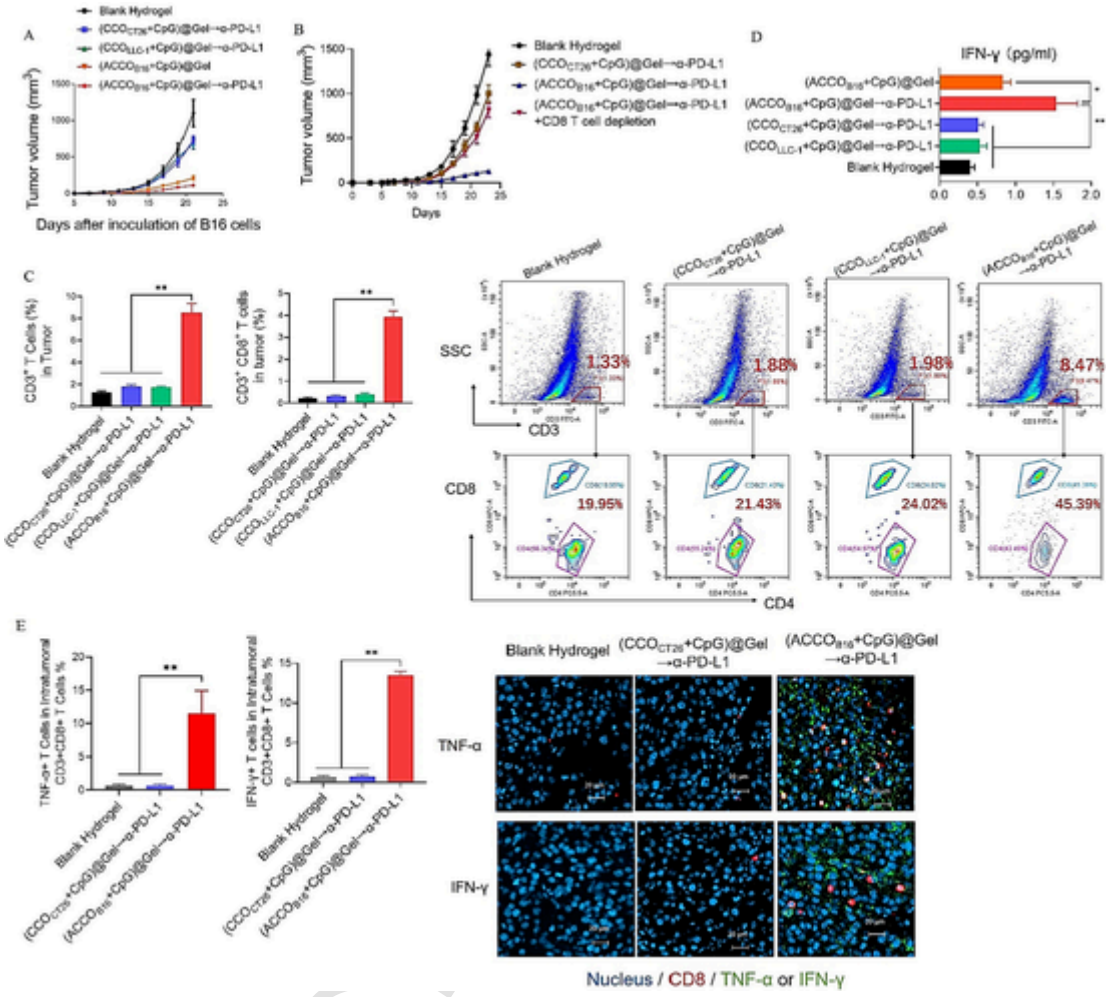

Fig. 5. Vaccines elicited antigen-specific antitumor effects. (A) Tumor growth curves of C57BL/6 mice receiving vaccines derived from autologous or non-autologous cancer cells and sequential three doses of α-PD-L1 therapy (n = 6). (B) Tumor growth curves of C57BL/6 mice receiving concurrent treatment of ($ACCO_{B16}$ + CpG)@Gel→α-PD-L1 and CD8+ T cell depleting antibody (250 μg per mouse, every 3 days for a total of four injections, n = 6). (C) Flow cytometry plots and proportions of tumor-infiltrating CD3+ T cells and CD3 + CD8+ T cells in vaccinated mice at day 21 (n = 6). (D) Intratumoral IFN-γ levels tested by ELISA kit (n = 6). (E) Immunofluorescence staining and flow cytometry analysis of CD8 + TNF-α + T cells and CD8 + IFN-γ + T cells in tumor (Scale bar, 20 μm). Statistical analysis was performed using one-way ANOVA; *$p < 0.05$, **$p < 0.01$.

Meanwhile, we also found that ($ACCO_{B16}$ + CpG)@Gel→α-PD-L1 had negligible impact on re-polarization of macrophages from tumor-promoting M2 phenotype to tumor-inhibiting M1 phenotype (Fig. S4). In addition, ($ACCO_{B16}$ + CpG)@Gel→α-PD-L1 also recruited immunosuppressive Tregs into the tumors, but still significantly increased the ratio of CD8+ T cells to Tregs (Fig. S5), thus reversing the immunosuppressive state. This was in consistence with the above result (Fig. 5B) that the anti-tumor effect of (ACCO + CpG)@Gel→α-PD-L1 largely depended on the CD8+ T cell activation.

3.6. Therapeutic efficacy against orthotopic colon carcinoma

Having demonstrated the effect of protective (ACCO + CpG)@Gel vaccine on potentiating α-PD-L1 to treat transdermally-accessible melanoma, we sought to evaluate whether this strategy could be broadly applicable to the treatment with orthotopic colon carcinoma which is difficult to access or perform surgery. BALB/c mice were pre-vaccinated with two subcutaneous injections of (ACCO + CpG)@Gel, in which ACCO was derived from colorectal CT26 cancer cells, and then challenged with orthotopic inoculation of CT26 cells in colon. With an identical trend, tumors orthotopically established in the colons of (ACCO + CpG)@Gel-vaccinated mice expressed higher level of PD-L1 (Fig. 6A). Afterward, mice were given three doses of α-PD-L1 intraperitoneally. Due to the inaccessibility of colon cancer, animal survival has become an important index to measure the therapeutic efficacy (Fig. 6B). Mice in blank control group died rapidly with the median survival of 20 days. In addition, unvaccinated mice with orthotopic colon cancer barely responded to α-PD-L1, and had a median survival of 22 days with no significance comparing to blank control. Significantly prolonged lifespan was observed in the orthotopic colon cancer models that had been vaccinated with (ACCO + CpG)@Gel (median survival of 32 days). Moreover, sequential treatment with α-PD-L1 further extended the median survival of (ACCO + CpG)@Gel-vaccinated mice to 38 days. To investigate whether (ACCO + CpG)@Gel→α-PD-L1 inhibited the progression of orthotopic colon cancer, histological analysis (Fig. 6C) and representative images (Fig. 6D) of excised colon from various groups were performed 10 days after tumor inoculation. As compared with the colon in tumor-free mice, tumor grow aggressively and extensively in the colons of mice from blank control and α-PD-L1 groups. In contrast, (ACCO + CpG)@Gel vaccination exerted protective effect against colon cancer and retard the tumor growth to some extent. And obviously, mice that were pre-vaccinated with (ACCO + CpG)@Gel and then treated with α-PD-L1 showed the strongest tumor inhibitory effect, as evidenced by the smallest colon tumor volume and distribution.

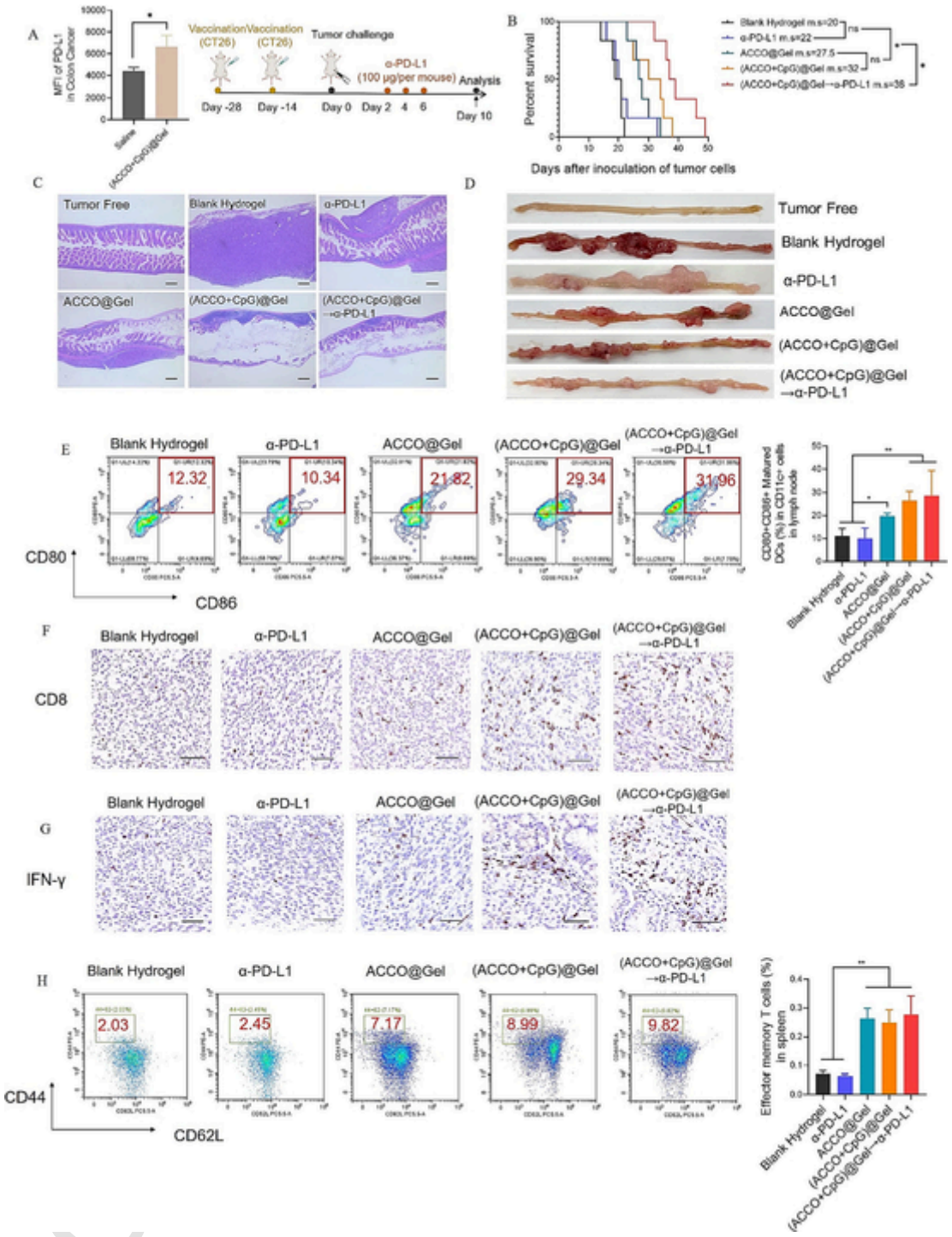

Fig. 6. Therapeutic efficacy of (ACCO + CpG)@Gel→α-PD-L1 against orthotopic colon carcinoma.(A) Intratumoral PD-L1 expression in vaccinated mice (n = 6) and schematic illustration of vaccination and α-PD-L1 antibody treatment schedule. (B) Survival curves of BALB/c mice after inoculation of CT26 cells (n = 6). (C) Histological assessment (scale bar, 200 μm) and (D) representative photographs of orthotopic colon tumor collected at day 10 after CT26 cells inoculation. (E) Flow cytometry plots and frequency of (CD80 + CD86 + CD11C +) matured DCs in lymph node at the endpoint. Immunohistochemical staining of colorectal cancers showing intratumoral (F) CD8 + T cell (scale bar, 50 μm) and (G) IFN-γ (scale bar, 50 μm) infiltration in colon cancers. (H) Flow cytometry analysis of (CD8 + CD44 + CD62L-) effector memory T cells in spleen (n = 6). Statistical analysis was performed using one-way ANOVA; *$p < 0.05$, **$p < 0.01$.

To confirm the immunization effect from (ACCO + CpG)@Gel, DC activation was assessed (Fig. 6E). As compared with unvaccinated mice from blank control and α-PD-L1 groups, vaccination with ACCO@Gel primed higher frequency of mature DCs (CD11c + CD80 + CD86 +) in lymph node, and this effect could be further boosted by additional CpG adjuvant of (ACCO + CpG)@Gel. As a result, considerably increased amount of CD8 + T cells were found to infiltrate the colorectal tumor tissue in (ACCO + CpG)@Gel-vaccinated mice (Fig. 6F), which created a favorable prerequisite for anti-PD-L1 therapy. Notably, (ACCO + CpG)@Gel→α-PD-L1 resulted in drastically increased density of CD8 + T cells and increased concentration of IFN-γ secreted by tumor-reactive T cells (Fig. 6G). Furthermore, the vaccinated mice from ACCO@Gel, (ACCO + CpG)@Gel and (ACCO + CpG)@Gel→α-PD-L1 groups all had significantly increased frequency of effector memory T

cells in spleen, indicating the establishment of anti-tumor immune memory against orthotopic colon cancer (Fig. 6H). Taken together, these results revealed that vaccination with (ACCO + CpG)@Gel could induce anti-tumor immune response to colorectal tumor, and the immunization effect could be further augmented by anti-PD-L1 therapy to delay the progression of orthotopic colon cancer.

3.7. Therapeutic efficacy against orthotopic lung carcinoma

We have also evaluated the reproducibility of the consecutive strategy combining prophylactic vaccination and ICB therapy in another refractory tumor model: orthotopic model of Lewis lung carcinoma. Similar schedule was applied as shown in Fig. 7A: C57BL/6 mice were pre-vaccinated with two subcutaneous injections of (ACCO + CpG)@Gel, in which ACCO was derived from LLC-1 cancer cells, then challenged with intravenous inoculation of LLC-1 cells, and afterward, given three doses of α-PD-L1 intraperitoneally. With an identical trend, tumors orthotopically established in the lungs of (ACCO + CpG)@Gel-vaccinated mice expressed higher level of PD-L1 (Fig. 6A). At day 16 after the tumor inoculation, histological analysis (Fig. 7B) and tumor nodules number count (Fig. 7C) of the lung lobe sections revealed that ACCO@Gel vaccination significantly decreased the pulmonary tumor nodules and achieved nearly 50% inhibition as compared with blank control. Additional CpG adjuvant further increased the immunization effect of (ACCO + CpG)@Gel against the growth of lung cancer with the inhibition rate of ~80%. Strikingly, while α-PD-L1 had no therapeutic impact in unvaccinated mice with pulmonary tumor, sequential treatment with α-PD-L1 almost completely prevented the establishment of orthotopic lung cancer in (ACCO + CpG)@Gel-vaccinated mice with nearly 100% inhibition rate. As a result, (ACCO + CpG)@Gel→α-PD-L1 showed the best capability of extending the animal survival time among the various treatments above (Fig. 7D).

Mechanism studies showed that (ACCO + CpG)@Gel-vaccinated mice from (ACCO + CpG)@Gel and (ACCO + CpG)@Gel→α-PD-L1 groups had considerably promoted amount of mature DCs in lymph node (Fig. 7E). Moreover, sufficient CD8 + T cells infiltration were observed in lungs of mice vaccinated with (ACCO + CpG)@Gel (Fig. 7F), which could benefit the ICB therapy. Intriguingly, the detected number of pulmonary CD8 + T cells in (ACCO + CpG)@Gel-vaccinated mice receiving α-PD-L1 therapy was low and approached near to a state similar to that of tumor free mice. This was probably because that (ACCO + CpG)@Gel→α-PD-L1 could generate effective effect to eradicate the orthotopic lung cancer. In addition, vaccination with ACCO@Gel, (ACCO + CpG)@Gel and (ACCO + CpG)@Gel→α-PD-L1 all resulted in a drastically higher frequencies of CD44 + CD62L− memory effector CD8 + T cells in spleen than unvaccinated mice (Fig. 7G),

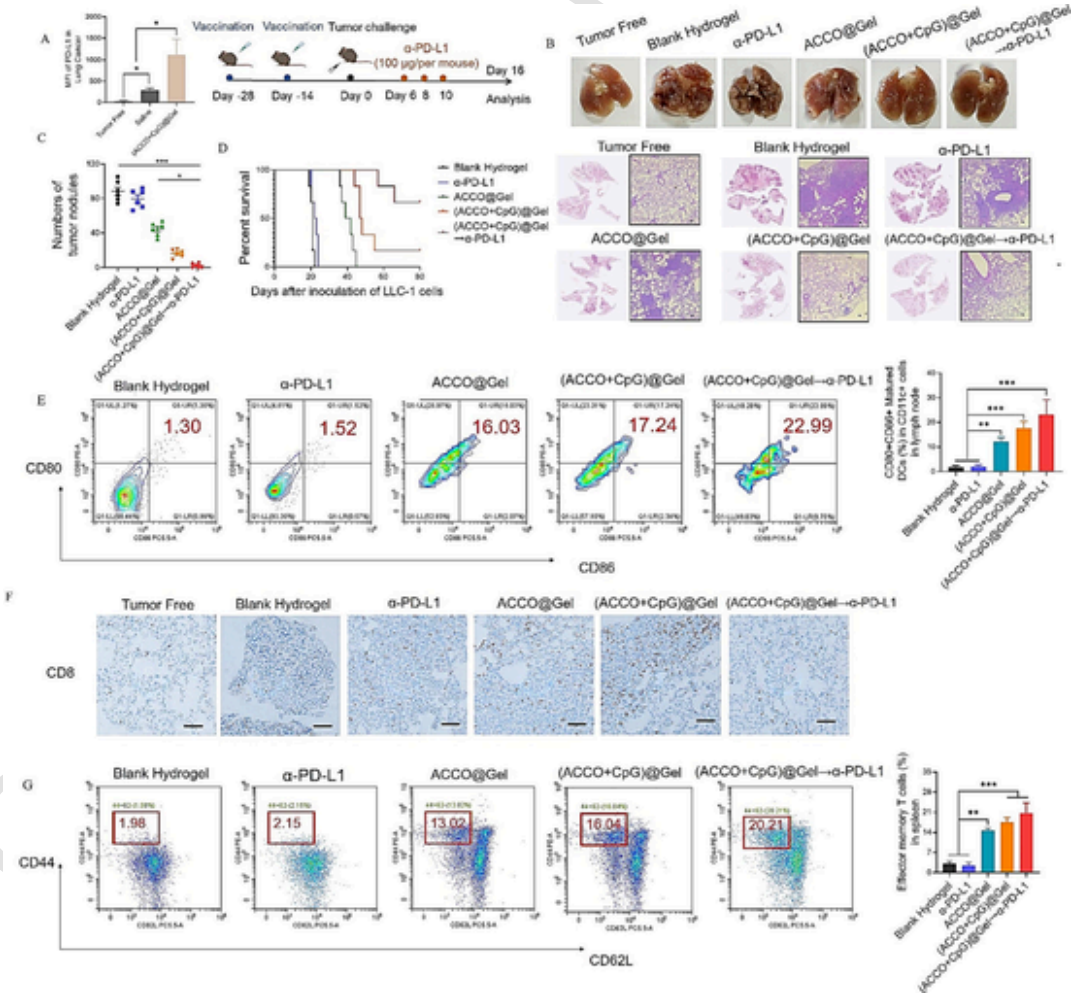

Fig. 7. Therapeutic efficacy of (ACCO + CpG)@Gel→α-PD-L1 against orthotopic lung carcinoma. (A) Intratumoral PD-L1 expression in vaccinated mice and schematic illustration of vaccination and α-PD-L1 antibody treatment schedule. (B) Representative photographs and H&E staining images of the lung tissue collected at day 16. Scale bars, 200 μm. Quantification of pulmonary tumor nodes (C) and survival percentage (D) of C57BL/6 mice pre-vaccinated with different vaccines (n = 6). (E) Flow cytometry plots and frequency of (CD80 + CD86 + CD11C +) matured DCs in lymph node at day 16 (n = 6). (F) Immunohistochemical analysis of CD8 + T cells in lung tissues at day 16 (n = 6). Scale bar, 100 μm. (G) Flow cytometry plots and frequency of effector memory T cells (gated on CD8 +) in the spleen examined at the same day (n = 6). Significance was calculated by one-way ANOVA. *P < 0.05, **P < 0.01, ***P < 0.001.

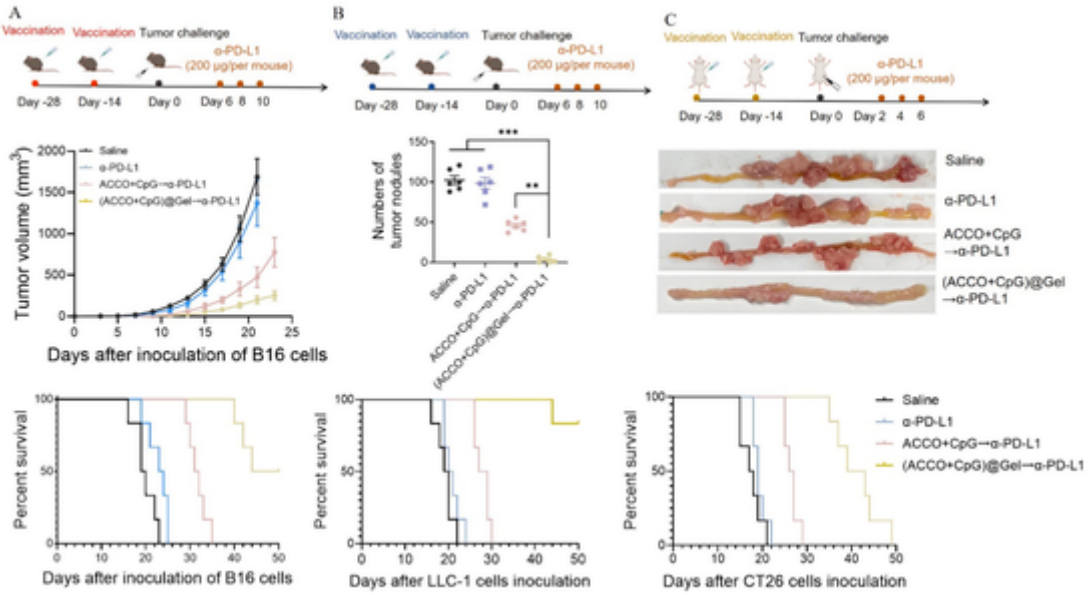

Fig. 8. (A) The arrow indicates the regimen schedule for (ACCO + CpG)@Gel→α-PD-L1 in melanoma cancer model. The dosage of α-PD-L1 applied here was 200 μg per mouse at Day 6, 8, and 10. Tumor growth and survival curves of mice with various vaccination and ICB treatments after B16 cells inoculation were recorded (n = 6). (B) The arrow indicates the regimen schedule for (ACCO + CpG)@Gel→α-PD-L1 in orthotopic model of lung cancer carcinoma. The dosage of α-PD-L1 was 200 μg per mouse at Day 6, 8, and 10. Numbers of tumor nodules in lung were counted at Day 16. Overall survival curves of vaccinated mice after LLC-1 cells inoculation were recorded (n = 6). (C) The arrow indicates the regimen schedule for (ACCO + CpG)@Gel→α-PD-L1 in orthotopic model of colon carcinoma. The dosage of α-PD-L1 was 200 μg per mouse at day 2, 4, and 6. Representative photographs of tumor progression in colon were collected at day 10. Overall survival curves of vaccinated mice after CT26 cells inoculation were recorded (n = 6). Statistical analysis was performed using one-way ANOVA; $^{**}p < 0.01$, $^{***}p < 0.001$.

which suggested the formation of anti-tumor immune memory *in vivo*. Collectively, in orthotopic lung cancer model, pre-vaccination with (ACCO + CpG)@Gel could elicit strong and durable anti-tumor immunity, which could be further enhanced by α-PD-L1 therapy to eliminate tumor cells.

3.8. Subcutaneous vaccination with ACCO and CpG incorporated in hydrogel produced better therapeutic outcome than free ACCO and CpG in suspension when combined with ICB

In another individual experiments, unvaccinated orthotopic models of melanoma, colon carcinoma, and lung carcinoma were treated with a doubling dosage of α-PD-L1. It was found that α-PD-L1 treatment with higher dose still failed to exert anti-tumor effect and showed comparable effects with saline groups, indicating that simply increasing the amount of α-PD-L1 given to unvaccinated mice resulted in minimal impact on enhancing tumor inhibition (Fig. 8). Since the anti-tumor principle for PD-L1 blockade therapies is to unleash the function of tumor-infiltrating T cells, the irresponsiveness to α-PD-L1 could be ascribed to the lack of pre-existing T cells in the tumors of unvaccinated mice. This result was also in contrast to above findings that α-PD-L1 even with a lower dose was able to elicit additional therapeutic effect in (ACCO + CpG)@Gel vaccinated models of orthotopic melanoma (Figs. 3 and 4), colon carcinoma (Fig. 6), and lung carcinoma (Fig. 7), again highlighting the significance of (ACCO + CpG)@Gel vaccination that could induce protective immunity, ameliorate the immune status and eventually render originally irresponsive tumors responsible to ICB therapy.

In addition, mice were also subcutaneously vaccinated with ACCO and CpG in the form of hydrogel or suspension, then challenged with orthotopic engraftment of autologous melanoma, colon carcinoma, or lung carcinoma, and treated with α-PD-L1 (Fig. 8). Previous studies had shown the minimal prophylactic or anti-tumor effect of ACCO [22] or CpG [35] in mice when subcutaneously vaccinated as free drug agents. In the current study, it was worth noting that, as compared with free ACCO and CpG with α-PD-L1 (ACCO + CpG → α-PD-L1), (ACCO + CpG)@Gel→α-PD-L1 showed superior effect on delaying the tumor progression and extending survival time (Fig. 8). Since extended release of cancer vaccine enables sustainable stimulation and amplifies *in vivo* bioactivities [22–24], this result highlights the necessity of using a hydrogel scaffold for controlled and sustained release of ACCO and CpG.

Thus, without the need for precise tumor targeting, a durable, protective, and tumor antigen-specific immune memory against certain types of intractable cancers can be built in advance by prophylactic administration of (ACCO + CpG)@Gel ahead of cancer occurrence to potentially prepare for (1) ameliorating the immune status of autologous tumors that are subsequently and orthotopically growing in vaccinated mice, and (2) rendering originally irresponsive tumors responsible to ICB therapy. Meanwhile, the time-staggered approach combining prophylactic (ACCO + CpG)@Gel vaccination and therapeutic ICB therapy before and after tumor occurrence could serve as a generalized framework to treat various types of orthotopic tumors growing in different regions that are, for various reasons, not suitable for targeted drug delivery, local administration or performing surgery.

3.9. Safety evaluation

To assess the safety of (ACCO + CpG)@Gel for *in vivo* application, we conducted safety evaluation in C57BL/6 mice and BALB/c mice that had received two doses of vaccination. As shown in Fig. 9A, during the vaccination period, no significant body weight drop was observed both in C57BL/6 mice and BALB/c mice. Meanwhile, in the healthy C57BL/6 mice model, no obvious abnormalities in the major organs including lung, liver, heart, kidney and spleen were observed after vaccination with (ACCO + CpG)@Gel (Fig. 9B), indicating no obvious toxicity.

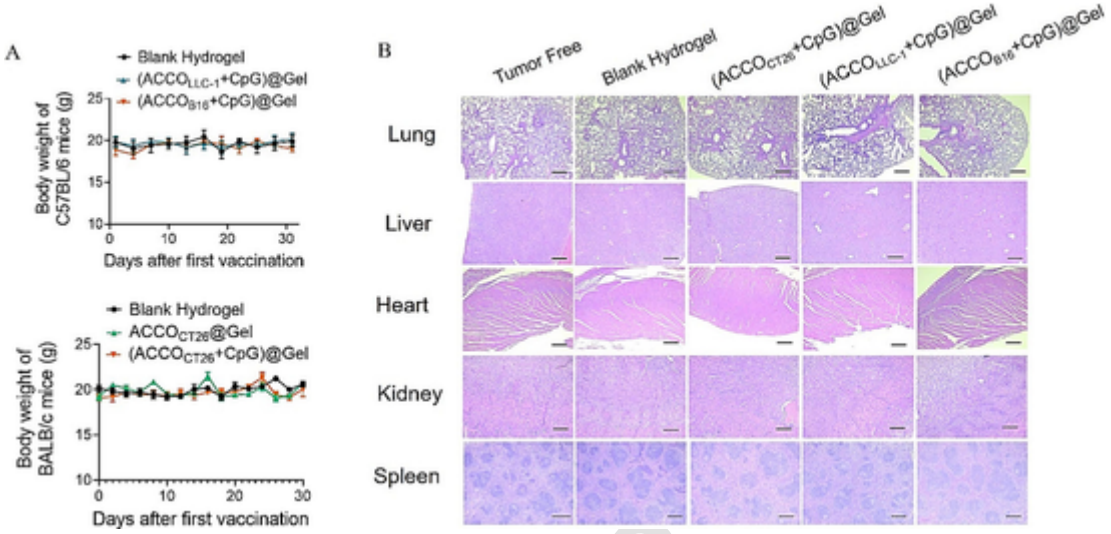

Fig. 9. *In vivo* safety evaluation. (A) Body weight changes in C57BL/6 and BALB/c mice after treatments with various vaccines. (B) H&E staining images of major organs (lung, liver, heart, kidney and spleen) at day 30 after vaccination. Scale bar, 50 μm.

4. Conclusion

In summary, we described an injectable hydrogel platform that simultaneously delivers immunogenic ACCO antigens and additional CpG adjuvants to function as protective vaccine by durably building tumor-specific immune memories against subsequent challenges with orthotopic tumors including melanoma, colon carcinoma, and lung carcinoma. Although vaccination with (ACCO + CpG)@Gel did not completely prevent the occurrence of these tumors, its immunization effect recruited substantial of tumor-reactive T cells to infiltrate into the occurrent tumors. Further treatment with α-PD-L1 significantly delayed the progression of tumor growth and prolonged the survival time of these orthotopic cancer models that originally did not respond to α-PD-L1 if unvaccinated. In conclusion, (ACCO + CpG)@Gel vaccination and ICB therapy have mutual interactions to reinforce each other: (1) (ACCO + CpG)@Gel could improve the immune status in tumors, thereby rendering tumor highly susceptible to ICB therapy; (2) ICB therapy could act as an amplifier of the anti-tumor immune response that was provoked by (ACCO + CpG)@Gel.

CRediT authorship contribution statement

Junlin Li : Conceptualization, Methodology, Formal analysis, Investigation, Writing – original draft. **Yue Yan :** Investigation, Methodology. **Ping Zhang :** Investigation. **Yun Jin :** Supervision. **Lian Li :** Conceptualization, Writing – original draft, Supervision, Funding acquisition.

Declaration of Competing Interest

The authors declare no competing financial interest.

Data availability

Data will be made available on request.

Acknowledgements

This work was supported by the National Natural Science Foundation of China (Grant No. 82104103).

Appendix A. Supplementary data

Supplementary data to this article can be found online at https://doi.org/10.1016/j.jconrel.2022.09.027.

References

[1] J.A. Seidel, A. Otsuka, K. Kabashima, Anti-PD-1 and anti-CTLA-4 therapies in cancer: mechanisms of action, efficacy, and limitations, Front. Oncol. 8 (2018) 00086.
[2] E.J. Lipson, P.M. Forde, H.-B. Hammers, L.A. Emens, J.M. Taube, S.L. Topalian, Antagonists of PD-1 and PD-L1 in cancer treatment, Semin. Oncol. 42 (4) (2015) 587–600.
[3] C. Boutros, A. Tarhini, E. Routier, O. Lambotte, F.L. Ladurie, F. Carbonnel, H. Izzeddine, A. Marabelle, S. Champiat, A. Berdelou, E. Lanoy, M. Texier, C. Libenciuc, A.M.M. Eggermont, J.-C. Soria, C. Mateus, C. Robert, Safety profiles of anti-CTLA-4 and anti-PD-1 antibodies alone and in combination, Nat. Rev. Clin. Oncol. 13 (8) (2016) 473–486.
[4] K.M. Mahoney, G.J. Freeman, D.F. McDermott, The next immune-checkpoint inhibitors: PD-1/PD-L1 blockade in melanoma, Clin. Ther. 37 (4) (2015) 764–782.
[5] J.M. Taube, A. Klein, J.R. Brahmer, H. Xu, X. Pan, J.H. Kim, L. Chen, D.M. Pardoll, S.L. Topalian, R.A. Anders, Association of PD-1, PD-1 ligands, and other features of the tumor immune microenvironment with response to anti-PD-1 therapy, Clin. Cancer Res. 20 (19) (2014) 5064–5074.
[6] A.C. Huang, M.A. Postow, R.J. Orlowski, R. Mick, B. Bengsch, S. Manne, W. Xu, S. Harmon, J.R. Giles, B. Wenz, M. Adamow, D. Kuk, K.S. Panageas, C. Carrera, P. Wong, F. Quagliarello, B. Wubbenhorst, K. D'Andrea, K.E. Pauken, R.S. Herati, R.P. Staupe, J.M. Schenkel, S. McGettigan, S. Kothari, S.M. George, R.H. Vonderheide, R.K. Amaravadi, G.C. Karakousis, L.M. Schuchter, X. Xu, K.L. Nathanson, J.D. Wolchok, T.C. Gangadhar, E.J. Wherry, T-cell invigoration to tumour burden ratio associated with anti-PD-1 response, Nature 545 (7652) (2017) 60–65.
[7] K.C. Soares, A.A. Rucki, A.A. Wu, K. Olino, Q. Xiao, Y. Chai, A. Wamwea, E. Bigelow, E. Lutz, L. Liu, S. Yao, R.A. Anders, D. Laheru, C.L. Wolfgang, B.H. Edil, R.D. Schulick, E.M. Jaffee, L. Zheng, PD-1/PD-L1 blockade together with vaccine therapy facilitates effector T-cell infiltration into pancreatic tumors, J. Immunother. 38 (1) (2015) 1–11.
[8] M. Zhou, C. Luo, Z. Zhou, L. Li, Y. Huang, Improving anti-PD-L1 therapy in triple negative breast cancer by polymer-enhanced immunogenic cell death and CXCR4 blockade, J. Control. Release 334 (2021) 248–262.
[9] L. Li, Y. Li, C.H. Yang, D.C. Radford, J. Wang, M. Janat-Amsbury, J. Kopecek, J. Yang, Inhibition of immunosuppressive tumors by polymer-assisted inductions of immunogenic cell death and multivalent PD-L1 crosslinking, Adv. Funct. Mater. 30 (12) (2020) 201908961.
[10] Y. Xiang, L. Chen, C. Liu, X. Yi, L. Li, Y. Huang, Redirecting chemotherapeutics to the endoplasmic reticulum increases tumor immunogenicity and potentiates anti-PD-L1 therapy, Small 18 (6) (2021) 2104591.
[11] L. Li, J. Wang, D.C. Radford, J. Kopecek, J. Yang, Combination treatment with immunogenic and anti-PD-L1 polymer-drug conjugates of advanced tumors in a transgenic MMTV-PyMT mouse model of breast cancer, J. Control. Release 332 (2021) 652–659.
[12] Y. Li, L. Li, J. Wang, D.C. Radford, Z. Gu, J. Kopecek, J. Yang, Dendronized polymer conjugates with amplified immunogenic cell death for oncolytic immunotherapy, J. Control. Release 329 (2021) 1129–1138.
[13] O. Kepp, A. Marabelle, L. Zitvogel, G. Kroemer, Oncolysis without viruses -

inducing systemic anticancer immune responses with local therapies, Nat. Rev. Clin. Oncol. 17 (1) (2020) 49–64.
[14] D. Zamarin, R.B. Holmgaard, S.K. Subudhi, J.S. Park, M. Mansour, P. Palese, T. Merghoub, J.D. Wolchok, J.P. Allison, Localized oncolytic Virotherapy overcomes systemic tumor resistance to immune checkpoint blockade immunotherapy, Sci. Transl. Med. 6 (226) (2014) 226ra32.
[15] S.J. Russell, K.-W. Peng, J.C. Bell, Oncolytic virotherapy, Nat. Biotechnol. 30 (7) (2012) 658–670.
[16] M. Garofalo, H. Saari, P. Somersalo, D. Crescenti, L. Kuryk, L. Aksela, C. Capasso, M. Madetoja, K. Koskinen, T. Oksanen, A. Makitie, M. Jalasvuori, V. Cerullo, P. Ciana, M. Yliperttula, Antitumor effect of oncolytic virus and paclitaxel encapsulated in extracellular vesicles for lung cancer treatment, J. Control. Release 283 (2018) 223–234.
[17] A. Ribas, R. Dummer, I. Puzanov, A. VanderWalde, R.H.I. Andtbacka, O. Michielin, A.J. Olszanski, J. Malvehy, J. Cebon, E. Fernandez, J.M. Kirkwood, T.F. Gajewski, L. Chen, K.S. Gorski, A.A. Anderson, S.J. Diede, M.E. Lassman, J. Gansert, F.S. Hodi, G.V. Long, Oncolytic Virotherapy promotes Intratumoral T cell infiltration and improves anti-PD-1 immunotherapy, Cell. 170 (6) (2017) 1109–1119.
[18] H.J. Chon, W.S. Lee, H. Yang, S.J. Kong, N.K. Lee, E.S. Moon, J. Choi, E.C. Han, J.H. Kim, J.B. Ahn, J.H. Kim, C. Kim, Tumor microenvironment remodeling by Intratumoral oncolytic vaccinia virus enhances the efficacy of immune-checkpoint blockade, Clin. Cancer Res. 25 (5) (2019) 1612–1623.
[19] A. Huang, M.M. Pressnall, R. Lu, S.G. Huayamares, J.D. Griffin, C. Groer, B.J. DeKosky, M.L. Forrest, C.J. Berkland, Human intratumoral therapy: linking drug properties and tumor transport of drugs in clinical trials, J. Control. Release 326 (2020) 203–221.
[20] Y. Zhou, T. Ye, C. Ye, C. Wan, S. Yuan, Y. Liu, T. Li, F. Jiang, J. Lovell, H. Jin, J. Chen, Secretions from hypochlorous acid-treated tumor cells delivered in a melittin hydrogel potentiate cancer immunotherapy, Bioact. Mater. 9 (2022) 541–553.
[21] C. Wan, Y. Sun, Y. Hu, J. Huang, L. Lu, Y. Gao, H. Zi, Q. He, J. Sun, J.F. Lovell, K. Yang, H. Jin, Peptide hydrogels loaded with irradiated tumor cell secretions enhance cancer immunotherapy, Nano Today 41 (2021) 101323.
[22] J. Li, P. Zhang, M. Zhou, C. Liu, Y. Huang, L. Li, Trauma-responsive scaffold synchronizing Oncolysis immunization and inflammation alleviation for post-operative suppression of Cancer metastasis, ACS Nano 16 (4) (2022) 6064–6079.
[23] C.G. Park, C.A. Hartl, D. Schmid, E.M. Carmona, H.J. Kim, M.S. Goldberg, Extended release of perioperative immunotherapy prevents tumor recurrence and eliminates metastases, Sci. Transl.Med. 10 (433) (2018) eaar1916.
[24] J. Liu, S.S. Liew, J. Wang, K.Y. Pu, Bioinspired and biomimetic delivery platforms for cancer vaccines, Adv. Mater. 34 (1) (2022) 2103790.
[25] H. Zhou, S. Forveille, A. Sauvat, T. Yamazaki, L. Senovilla, Y. Ma, P. Liu, H. Yang, L. Bezu, K. Mueller, L. Zitvogel, O. Rekdal, O. Kepp, G. Kroemer, The oncolytic peptide LTX-315 triggers immunogenic cell death, Cell Death Dis. 7 (2016) e2134.
[26] Y. Xia, J. Wei, S. Zhao, B. Guo, F. Meng, B. Klumperman, Z. Zhong, Systemic administration of polymersomal oncolytic peptide LTX-315 combining with CpG adjuvant and anti-PD-1 antibody boosts immunotherapy of melanoma, J. Control. Release 336 (2021) 262–273.
[27] B. Haug, K. Camilio, L. Eliassen, W. Stensen, J. Svendsen, K. Berg, B. Mortensen, G. Serin, J. Mirjolet, F. Bichat, O. Rekdal, Discovery of a 9-mer cationic peptide (LTX-315) as a potential first in class oncolytic peptide, J. Med. Chem. 59 (7) (2016) 2918–2927.
[28] J.J. Wei, D. Wu, S. Zhao, Y. Shao, Y. Xia, D. Ni, X. Qiu, J. Zhang, J. Chen, F. Meng, Z. Zhong, Immunotherapy of malignant glioma by noninvasive administration of TLR9 agonist CpG nano-immunoadjuvant, Adv. Sci. 9 (13) (2022) 2103689.
[29] K. Kigasawa, K. Kajimoto, T. Nakamura, S. Hama, K. Kanamura, H. Harashima, K. Kogure, Noninvasive and efficient transdermal delivery of CpG-oligodeoxynucleotide for cancer immunotherapy, J. Control. Release 150 (3) (2011) 256–265.
[30] M. Zhou, Q. Zuo, Y. Huang, L. Li, Immunogenic hydrogel toolkit disturbing residual tumor "seeds" and pre-metastatic "soil" for inhibition of postoperative tumor recurrence and metastasis, Acta Pharm. Sin. B 12 (8) (2022) 3383–3397.
[31] Y. Xiang, L. Chen, L. Li, Y. Huang, Restoration and enhancement of immunogenic cell death of cisplatin by Coadministration with digoxin and conjugation to HPMA copolymer, ACS Appl. Mater. Inter. 12 (1) (2020) 1606–1616.
[32] H. Ruan, Q. Hu, D. Wen, Q. Chen, G. Chen, Y. Lu, J. Wang, H. Cheng, W. Lu, Z. Gu, A dual-bioresponsive drug-delivery depot for combination of epigenetic modulation and immune checkpoint blockade, Adv. Mater. 31 (17) (2019) e1806957.
[33] C. Wang, J. Wang, X. Zhang, S. Yu, D. Wen, Q. Hu, Y. Ye, H. Bomba, X. Hu, Z. Liu, G. Dotti, Z. Gu, In situ formed reactive oxygen species-responsive scaffold with gemcitabine and checkpoint inhibitor for combination therapy, Sci. Transl. Med. 10 (429) (2018) eaan3682.
[34] R. Kuai, W. Yuan, S. Son, J. Nam, Y. Xu, Y. Fan, A. Schwendeman, J.J. Moon, Elimination of established tumors with nanodisc-based combination chemoimmunotherapy, Sci. Adv. 4 (4) (2018) eaao1736.
[35] R. Kuai, X. Sun, W. Yuan, L.J. Ochyl, Y. Xu, A.H. Najafabadi, L. Scheetz, M. Yu, I. Balwani, A. Schwendeman, J.J. Moon, Dual TLR agonist nanodiscs as a strong adjuvant system for vaccines and immunotherapy, J. Control. Release 282 (2018) 131–139.